This article has been accepted for publication in a future issue of this journal, but has not been fully edited. Content may change prior to final publication. Citation information: DOI 10.1109/TMI.2019.2951439, IEEE Transactions on Medical Imaging

Automatic Diagnosis Based on Spatial Information Fusion Feature for Intracranial Aneurysm

Yuwen Zeng, Xinke Liu, *Member, IEEE,* ✉Nan Xiao, *Member, IEEE* Youxiang Li, Yuhua Jiang, Junqiang Feng, Shuxiang Guo, *Senior Member, IEEE*

***Abstract*—Timely and accurate auxiliary diagnosis of intracranial aneurysm can help radiologist make treatment plans quickly, saving lives and cutting costs at the same time. At present Digital Subtraction Angiography (DSA) is the gold standard for the diagnosis of intracranial aneurysm, but as radiologists interpret those imaging sequences frame by frame, misdiagnosis might occur. The utilization of computer-assisted diagnosis (CAD) can ease the burdens of radiologists and improve the detection accuracy of aneurysms. In this paper, a deep learning method is applied to detect the intracranial aneurysm in 3D Rotational Angiography (3D-RA) based on a spatial information fusion (SIF) method, and in stead of 3D vascular model, 2D image sequences are used. Given the intracranial aneurysm and vascular overlap having similar feature in the most time, rather than focusing on distinguishing them in one frame, the morphological differences between frames are considered as major feature. In the training data, consecutive frames of every imaging time series are extracted and concatenated in a specific way, so that the spatial contextual information could be embedded into a single two-dimensional image. This method enables the time series with obvious correlation between frames be directly trained on 2D convolutional neural network (CNN), instead of 3D-CNN with huge computational cost. Finally, we got an accuracy of 98.89%, with sensitivity and specificity of 99.38% and 98.19% respectively, which proves the feasibility and availability of the SIF feature.**

***Index Terms*—Intracranial aneurysm, computer-assisted diagnosis, spatial information fusion, deep learning.**

I. Introduction

Intracranial aneurysm (IA), is a swelling part on an artery in the brain. Intracranial aneurysm is the main cause of subarachnoid haemorrhage, and its morbidity is next to the hypertensive cerebral hemorrhage and thrombosis [1]. Because there are usually no obvious symptoms when an aneurysm forms, about 80% to 90% aneurysms are found after it ruptured [2]. Therefore, timely and accurate treatment is indispensable.

So far, Computed Tomographic Angiography (CTA), Magnetic Resonance Angiography (MRA), and Digital Subtraction Angiography (DSA) are regarded as the diagnosis and treatment approaches [3][4]. CTA is a non-invasive volumetric imaging technique that does not require arterial puncture or catheter manipulation. However, the specificity and sensitivity could be low on small aneurysm in the hindbrain. MRA is a non-invasive and non-radiative imaging technique. Whereas deficiencies are that patients with metal in their bodies cannot use MRA, and its detection accuracy is inferior to DSA due to the low resolution [5]. DSA is suitable as an interventional imaging technique, contrary to CTA and MRA, and therefore can be applied during treatment. It has a relatively high sensitivity and specificity for aneurysm detection, and can steadily depict the spatial location of aneurysms [6]. On the other hand, the radiation affects both patients and surgeons because vascular interventional surgery must be carried out to apply contrast and even endovascular bypass.

Imaging techniques yield a great deal of information that radiologists or other medical professionals have to analyze and evaluate comprehensively in a short time. To relieve them from repeating hard work and improve the accuracy of aneurysm detection, computer-assisted diagnosis (CAD) can assist doctors in the interpretation of medical images [7][8]. CTA is fast, non-invasive, and relatively inexpensive and MRA is radiation-free and non-invasive. Radiologists use them in many instances. Then they analyze these images to determine the location and size of the aneurysm. However, DSA is still considered the gold standard for cerebral aneurysm diagnosis. If any interventional therapy is needed, then there would be more data to process. Radiologists need to perform angiography on main intracranial arteries, and interpret the angiographic sequences frame by frame, which is a great burden. Such repetitive work can lead to mind fatigue and even misdiagnosis [9].

Therefore, the introduction of CAD system is significative. It firstly reduces the redundant information in the imaging sequences, processes the medical image systematically and finally combines the original imaging sequences with useful information. The result is then screened by the radiologist for rapid and accurate diagnosis. This saves time and im-

Manuscript received May 15, 2019; first revised September 16, 2019; second revised October 15; accepted October 29. This work was supported by the National Key Research and Development Program of China (No.2017YFB134401). (Corresponding author: N. Xiao)

Y. Zeng, N. Xiao are with the School of Life Science, Beijing Institute of Technology, Beijing, China.

X. Liu, Y. Li, Y. Jiang and J. Feng are with the Department of Interventional Neuroradiology, Beijing Neurosurgical Institute and Beijing Tiantan Hospital, Capital Medical University, Beijing, China.

S. Guo is with the School of Life Science, Beijing Institute of Technology, Beijing, China, and Faculty of Engineering, Kagawa University, 2217-20 Hayashi-cho, Takamatsu, Kagawa, Japan.

Y. Zeng and X. Liu contributed equally to this study.

This article has been accepted for publication in a future issue of this journal, but has not been fully edited. Content may change prior to final publication. Citation information: DOI 10.1109/TMI.2019.2951439, IEEE Transactions on Medical Imaging

proves diagnostic accuracy. It is noteworthy that the CAD is definitely not going to replace the radiologist or other medical professional, indeed it can be an efficient assistant.

In this paper, we present a fully-automatic intracranial aneurysm detection method based on spatial information fusion (SIF) method. Instead of using the 3D vascular model that reconstructed from the 3D-Rotational Angiography (3D-RA), we chose the original 3D-RA projection images. There are three reasons in total. Firstly, 3D reconstruction needs threshold segmentation which will significantly affect the measurement results [10]. The selection of Hounsfield Unit (HU) thresholds may influence the size of the measured aneurysm, whereby lower a HU threshold could artificially make vessels appear larger and vice versa. Furthermore, as is widely reported that the sizes of aneurysm necks that could be measured on 2D-DSA tended to be smaller compared to 3D reconstructed DSA [11][12], so in our clinical practice, we combine the 2D-DSA and 3D-DSA to get a more comprehensive assessment for intracranial aneurysms. Secondly, 3D-CNN is not mature enough since the computation and memory requirements are very huge. Finally, this method might also provide reference for some other recognition tasks on 2D images or videos. Since the sequences of 3D-RA consists of a series of 2D images that were obtained by scanning head around, there is a certain projection angle relationship between the front and rear frames. On the basis of traditional batch-based classification method, we embedded the spatial information into a single image by concatenating the consecutive frames, so that the aneurysm can be distinguished from the curve of vessels or overlap between vessels which are very similar to the aneurysm. The rest of this paper is organized as follows: Section II describes the current state-of-the-art by citing related research work and Section III provides a detailed overview of proposed computer-aided aneurysm diagnosis method. Section IV presents experimental results and performance evaluation of our proposed framework in terms of robustness and efficiency. Finally, Section V concludes the paper and highlight some future directions.

II. Related work

There are already many studies on CAD systems, especially on microscopic pathology image. The most commonly used methods are machine learning. Support vector machines (SVM) and random forest (RF) are used in predicting non-small cell lung cancer prognosis [13]. Deep belief network (DBN) and haar-wavelet were applied to detect mammographic masses [14]. Convolutional neural network (CNN) was developed for detection on lymph node, breast cancer [15], prostatic cancer [16], brain tumour [17], brainstem gliomas [18], and melanoma [19]. Besides these image-based method, CNN also had an excellent performance on medical image aynthesis with adversarial learning strategy [20]. Accuracy about 90%-95% rate was achieved in the classification and grading of breast cancer, brain tumor and prostate cancer. 3D-CNN with high computational overhead obtained high accuracy likewise on pulmonary nodule detection [21]. As for intracranial aneurysm, a large portion of studies focused on semi-automatic or automatic aneurysm CAD system for aneurysm detection and morphological analysis [22][23] through MRA and CTA rather than DSA. The main reason is that MRA and CTA data can be viewed from different projection angle in both 2D and 3D modes. The 3D vascular model that is reconstructed from the 3D-RA data includes more spatial information but it requires more advanced hardware, and larger doses of radiation. However, despite that DSA is gold standard of intracranial aneurysm detection and rupture risk quantification, it still remains less researched, which we suppose 2D images and difficulties on obtaining available dataset might contribute to the reasons.

Miki *et al*. [24] evaluated the CAD in a routine reading environment. The use of the CAD system increased the number of detected aneurysms by 9.3%. Takahiro *et al*. [25] analysed different indicators of aneurysms, such as size, location, patients gender and age, and come to the conclusion that the size of aneurysm had significant influence to the detection results. Those aneurysms with more than 4-5 mm in diameter reached almost 100% accuracy. As the size decreases, the detection accuracy would greatly reduce. It might also be related to the resolution of the MRA imaging.

Clemens M. *et al*. [26] proposed a system to detect intracranial aneurysm in 3D-RA, MRA and CTA based on blob-enhancing filter. The method was tested on 65 angiography sequences. Finally they achieved 96% sensitivity with 2.6 FP/ds (false positive per data set) in 3D-RA, 94% sensitivity with 8.0 FP/ds in MRA and 90% sensitivity with 28.1 FP/ds in CTA. Whereas their high sensitive came at the expense of false positive rate.

Jerman *et al*. [27] applied detection using random decision forests with hand-crafted feature. On 10 restructed 3D vessel containing 15 aneurysms, the proposed method achieved a 100% sensitivity at 0.4 FP/ds. However,the small data set means it can be incomplete for all kinds of aneurysms. So later they proposed an automatic way to detect saccular aneurysms in restructed 3D vessel [28], where a spherical and elliptical structure enhancing filter was followed by a 2D-CNN. However, the same problem about simplex and tiny data set still existed.

Ines Rahmany *et al*. [29] proposed a 2D-DSA intracranial aneurysm detection system based on the fusion of two fuzzy classifiers. The idea of segmenting the vascular tree by Fuzzy C-Means (FCM) and Fuzzy K-Nearest Neighbor (FKNN) is convincing, but the reliability of the system is questionable because the number of training data is not mentioned, and the final result is without detailed explanation. The same problem occurred on paper [30], sensitivity 100% with 1.85 FPs (false positive cases) per patient was obtained on 7 aneurysms by using gradient concentrate filter in MRA. Malik *et al*. [31] proposed an intracranial aneurysm detection framework on 2D-DSA which achieved high accuracy of 98% for classification. A total of 47 aneurysms from 59 angiographic sequences were used. Each sequence was rel-

This article has been accepted for publication in a future issue of this journal, but has not been fully edited. Content may change prior to final publication. Citation information: DOI 10.1109/TMI.2019.2951439, IEEE Transactions on Medical Imaging

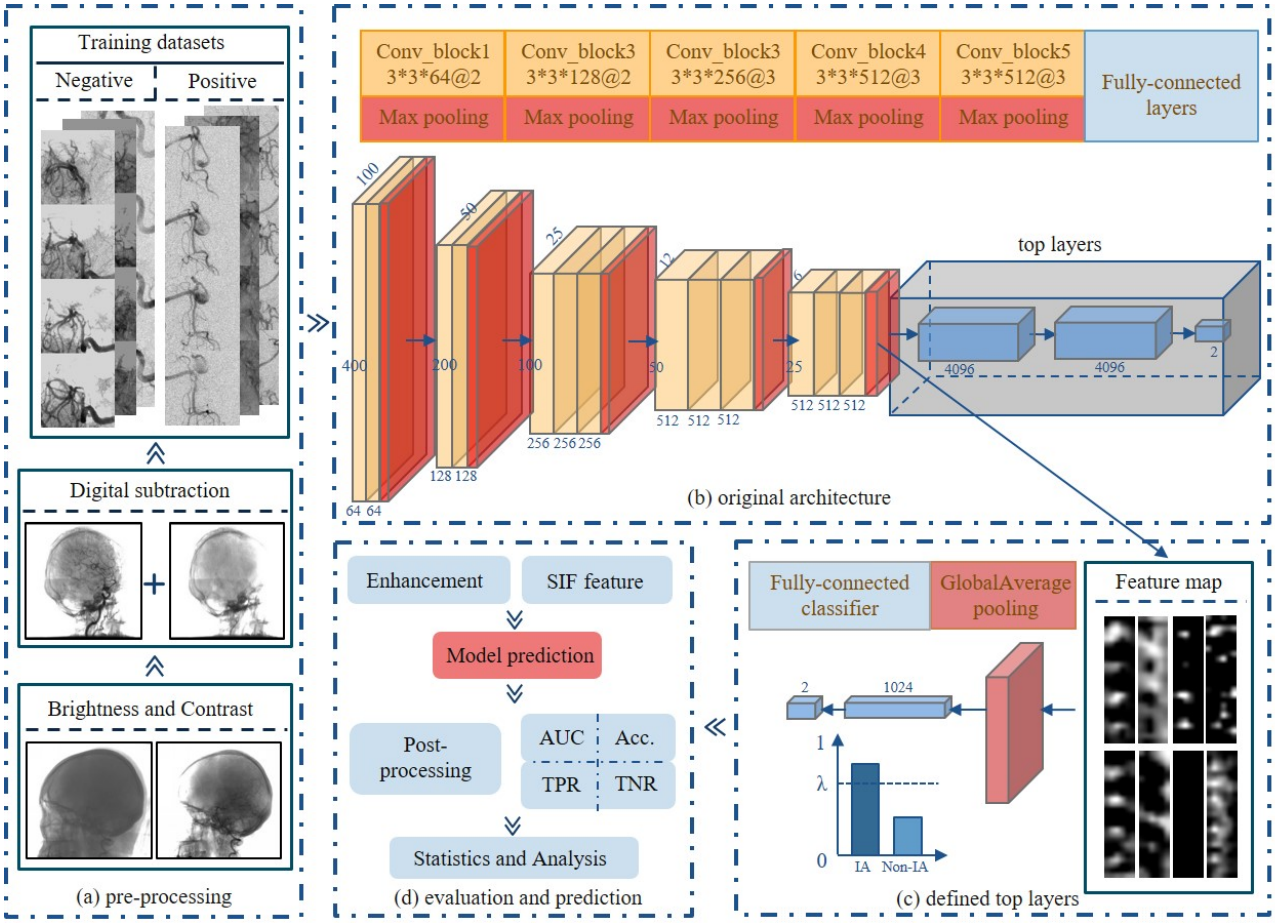

Fig. 1: Flowchart of the proposed framework for computer-aided intracranial aneurysm detection system. (a) shows the pre-processing for original imaging sequences. (b) Architecture of convolutional neural network, VGG16 was used for transfer learning. (c) Adjustment on network. The original top layers were replaced with new pooling and fully-connected layers. (d)Model evaluation and prediction.

atively clear and the size range of aneurysms was between 6mm and 21mm, but there is no discription on distribution of aneurysm diameter.

We therefore conclude that most of the existing studies on intracranial aneurysm detection are conducted on the basis of 3D data obtaining from CTA, MRA, and 3D-DSA. Among them, the most commonly used method is the spherical filter [32][33], which is then classified by decision forest or CNN. Little comprehensive effort has been devoted to 2D-DSA or 3D-RA that is not reconstructed, although DSA is the gold standard for aneurysm diagnosis. Methods such as FCM, distance transformation and multi-layer perceptron (MLP) have achieved good results, but there still exist two unavoidable problems. One is the small amount of training and test data, and the other is that the size of aneurysms is limited to a narrow range. Both lead to insufficient representation and generalization of CAD system.

III. Design of the Aneurysm Detection System

Due to the excellent performance of deep learning models in natural language process and computer vision, it has been gradually valued in biomedical informatics [34][35]. Most convolutional neural networks use single original or clipped images as training data, and some use feature maps to further improve the convergence speed and accuracy. These methods are very useful for target recognition and classification task, but it cannot effectively identify targets in video sequence, which is mainly because of the loss of spatial or temporal relationship between frames. To improve that, rather than feeding single image, we fuse the spatial information of consecutive frames into a two-dimensional image to reserve the third dimensional feature.

A. Pre-processing

As the two images at the bottom of Fig. 1(a) show, the original dicom data on the left is almost black and no blood vessels are visible in the image. So we perform Gamma Correction on the original image and then stretch or shrink its intensity to right levels. The original data are unsubtracted

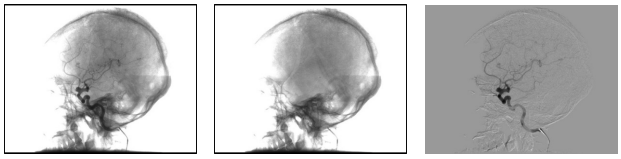

(a) (b) (c)

Fig. 2: Example of unsubtracted, pre-contrast, and digital subtraction image.

X-ray sequences for blood vessels in a bony or dense soft tissue environment, which are produced using contrast

This article has been accepted for publication in a future issue of this journal, but has not been fully edited. Content may change prior to final publication. Citation information: DOI 10.1109/TMI.2019.2951439, IEEE Transactions on Medical Imaging

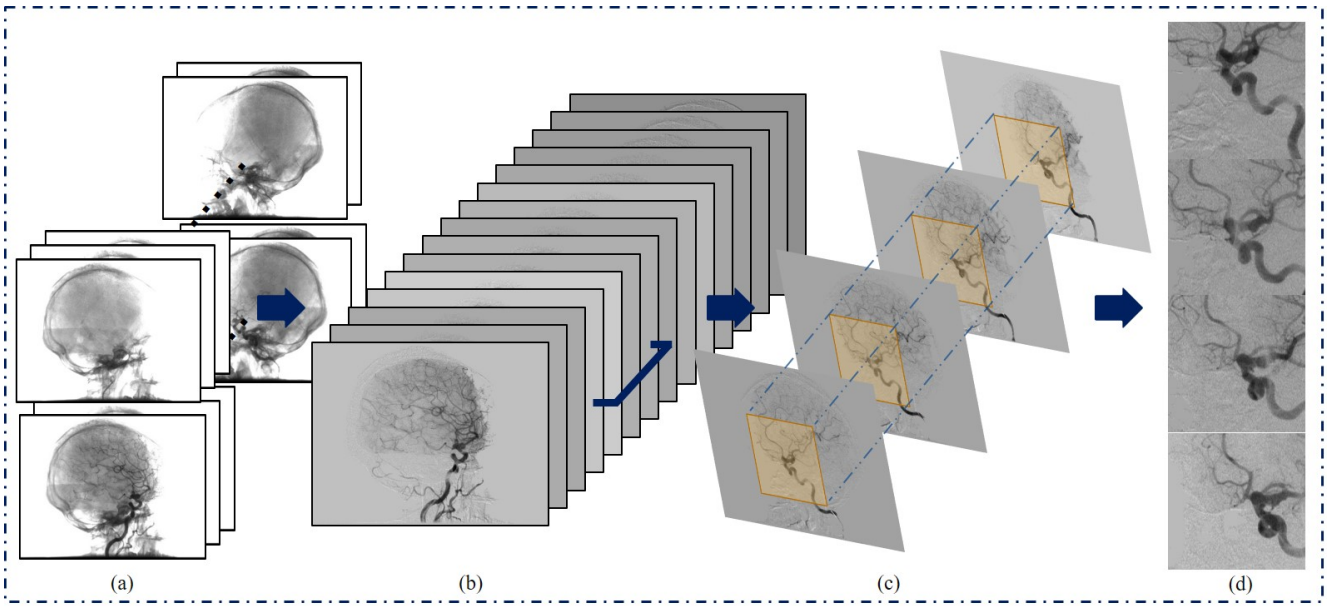

Fig. 3: Demonstration of spatial information fusion method. Original sequences (a) of contrast and un-contrast data were used to generate digital subtraction angiography data (b). (c) A certain amount of ROIs were extracted from consecutive frames and then concatenated as the training data (d).

medium. The images are useful for determining anatomical position and variations, but unhelpful for visualizing blood vessels. Therefore, we applied digital subtraction to the original data by the pre-contrast sequences. The obtained images are the same as DSA as shown in Fig. 2.

To reduce the noise in the fluoroscopic images, the median filter is applied to remove noise and smooth every single frame [28][31]. Since there is no reference image, we measure the filters in terms of the Signal to Noise Ratio (SNR). With the lowest score of bilateral filter as the normalization criterion, the median, gaussian and bilateral filter scores are 1.0294, 1.0282 and 1.0046 respectively.

B. Spatial information fusion(SIF)

A simple two-dimensional image contains plane information, including edges, textures, colors, lines and other factors, whereas a 3D model represents the shape established by the surface information of an object, with the object itself as the center of the coordinate system. And from the perspective of the observer, it is possible to observe the same object from different directions and obtain the previously blocked surface information within a certain range. This is a 2.5D description of the target which we applied in this method, similar to the principle of binocular or multi-camera calibration. The traditional method of training network with single image will lose the information between frames. Taking part of features as a whole may lead to the decrease on accuracy. This would have few impact on the object recognition and classification task in daily life, whereas in the angiography, the features of vascular curve and overlap are very similar to aneurysms. When these structures are in the same frame, it is prone for CNN to ignore the characteristics of the trend of blood vessels around aneurysms and misclassify them. If it is an overlap between vessels or a sudden curve of vessel, the imaging of it shall gradually disappear with the change of angiography angle but aneurysms will not. As shown in the Fig. 4, the overlaps are marked in blue, and the aneurysms are marked in red. With viewpoint changing, the shadow of vascular overlaps would fade, disappear or even appear again, but aneurysms barely changed.

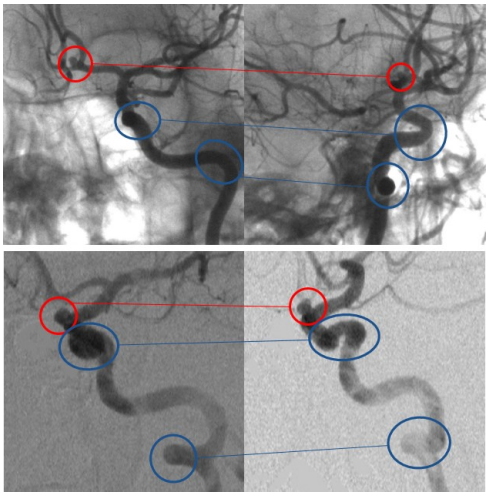

Fig. 4: Demonstration of vascular overlaps and aneurysms with different viewpoint. First row is non-subtraction image, and second row is subtraction imgae. Aneurysms are marked in red circle and vascular overlaps are marked in blue circle.

Although there have been studies on the application of 3D-CNN to the behavior recognition of video monitoring, the amount of parameters of 3D-CNN is so much that it cannot be widely used at present. Therefore, we consider to fuse the spatial information from the time series into single image, so that the two-dimensional image could contain the contextual information in the series. Though imageing sequence consists of two-dimensional image data, it can also be regarded as three-dimensional data if we take time or projection angle into account. As depicted in Fig. 3, the

This article has been accepted for publication in a future issue of this journal, but has not been fully edited. Content may change prior to final publication. Citation information: DOI 10.1109/TMI.2019.2951439, IEEE Transactions on Medical Imaging

imaging sequence can be expressed as follows:

$$i(N) = \{i_1^0, i_2^\theta, i_3^{2\theta}, ..., i_N^{(N-1)\theta}\} \tag{2}$$

where θ is the difference of angiography angle between each frame, i_n^α represents the nth frame with viewing angle $\alpha = n\theta$, then $i_{n+m}^{\alpha+m\theta}$ represents the mth frame after i_n^α with viewing angle $\alpha + m\theta$. Note that the angle difference between frames is not a constant value because of the acceleration and deceleration of the machine at the beginning and end of the rotational scan. And this method is not sensitive to the angular change since the SIF feature is composed of the special information brought by the angle difference. Each frame in the sequence can be seen as a different angle projection of the 3D blood vessel model. Finally we denoised each frame, extract m regions of interest (ROIs) from every l consecutive frames and concatenate them vertically into a single image $SIF - m$:

$$i_n^\alpha(\mathrm{x}_0,\mathrm{y}_0) - i_{n+ml}^{a+ml\theta}(\mathrm{x}_0,\mathrm{y}_0) \tag{3}$$

where $(\mathrm{x}_0,\mathrm{y}_0)$ is the central coordinate of the i_n^a. Notice that the m successive regions of interest (ROIs) have the same central coordinate, which means their spatial positions are constant on the timeline. In this case, the aneurysm will not always be at the center of the image, but will be shifted to a certain extent as the angle changes, and might disappear in the latter ROIs.

C. Model Selection

Deep learning paradigms are used for feature extraction and transfer learning [36]. Since these networks are deep, complex in structure and have a large number of parameters, it takes a lot of time to train a network from scratch. Meanwhile superficial layer of CNN learns the basic structure of the image, such as color and edge features, which are common features of things, whereas the deeper layer of network learns the abstract features of the image, such as the wheels of a car, the eyes of a person, or aneurysms in the intracranial blood vessels. Therefore, we froze the shallow layer of networks and keep the weight parameters of these layers untrainable, only the specified layers were trained.

TABLE I: INITIAL TEST RESULTS OF CNN PARADIGMS

Model	Training Acc.	Valid Loss	Test Acc.
$VGG16$	94.31	27.8	91.12
$ResNet50$	89.1	61.6	51.23
$InceptionV3$	83.38	51.7	65.67
$DenseNet121$	91.52	38.6	87.45

VGG16, ResNet50, InceptionV3 and DenseNet121 are outstanding in the field of computer vision, so an initial test are conducted to select the appropriate model for this task. Non-augmented SIF-3 features were used as the data set. As the TABLE I shows, VGG16 is chosen for its better and steady performance. Other models have achieved good or even better results in ImageNet, but complex structures lead to overfitting or just hard to converge. In fact, despite the large number of VGG16 parameters, nearly 110M of them come from the two large full-connection layers at the top of the network. So we only maintained the architecture of models that do not include the top layers. Then on the top of the last convolutional layer, we added a global average pooling layer, followed by a fully-connected layer with ReLU and the final classification layer with Softmax. The categorical cross-entropy loss was used as minimization objective function. Assuming that the distribution of ground truth label is p and the distribution of label from the model output is q, then the cross-entropy of them on the given data set X is $CE(p,q) = -\sum_{x \in X} p(x) \log q(x)$. Stochastic gradient descent (SGD) was chosen as the optimization technique with initial learning rate of 10^{-4}. Momentum and Nesterov term were used to suppress oscillation and accelerate convergence, and to provide a correction during gradient updates while increasing sensitivity, respectively.

D. Data set

In vascular interventional surgery, X-ray was cast $180°$ around patients' head, from the right side to the back and finally to the left side. We acquired 300 original sequences with 263 aneurysms from Beijing Tiantan Hospital, China. A waiver was obtained from Beijing Tiantan hospital ethic board. The original data contained 133 frames per sequence, with an average inter-frame angle difference $1.36°$. 15 uniformly distributed frames of each original sequences were picked out by radiologists and then the ground truth of aneurysm was performed by 5 professional radiologists. Due to the large angle difference, aneurysms on the further branch are more likely to be lost in the latter ROIs. As shown in Fig. 5, r_1 and r_2 are the perpendicular distance to the center of brain. θ is the angle difference of imaging machine. w_1 and w_2 are the window width of ROIs. This diagram is on transverse plane, namely viewing from the top of the head to the feet. A is an proximal aneurysm on artery and B is an distal aneurysm on branch. As the X-ray machine rotates, aneurysm B at the distal end of the branch travels a longer distance on the circle, which is $BB_1 > AA_1$. So there exists the following relationship:

$$w_1 = r_1(1 - \sin\theta) < w_2 = r_2(1 - \sin\theta)$$

In other words, to see both B and B1 from the coronal plane, we need a larger window width than that for A and A1.

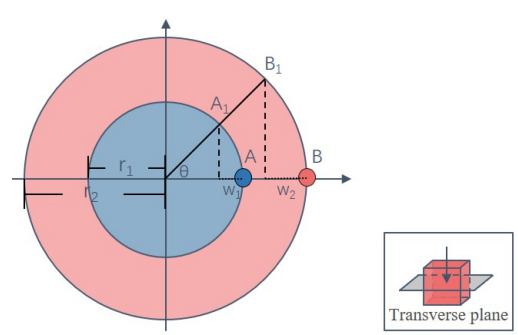

Fig. 5: Schematic plan of field angle of aneurysms on artery(A) and on branch(B).

This article has been accepted for publication in a future issue of this journal, but has not been fully edited. Content may change prior to final publication. Citation information: DOI 10.1109/TMI.2019.2951439, IEEE Transactions on Medical Imaging

Therefore, in the original 133-frame sequences, the average inter-frame angle difference of $1.36°$ could ensure the presence of aneurysms in the selected ROIs. However, it is precisely because of the small angle difference, the adjacent images are almost unchanged, and it is difficult to distinguish

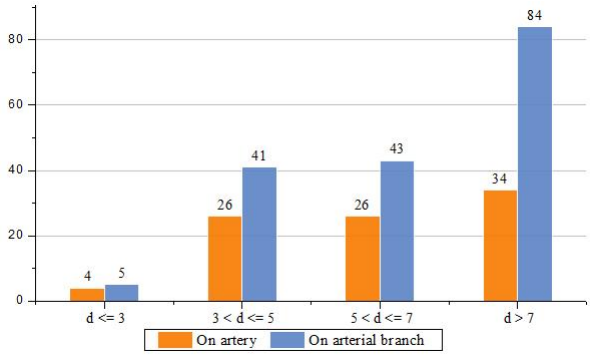

Fig. 6: Distribution of diameters(d) of aneurysms on artery and arterial branch.

the aneurysm from the vascular overlap and corner. This will cause a lot of redundant computing, not conducive to the improvement of accuracy. The inter-frame difference of the training data selected by the radiologist is suitable to observe the changes in vascular structure. But the more the ROI in a SIF image is, the more likely the aneurysm in the latter ROI will disappear.

There are 263 aneurysms in total. The diameters of them range from 1.8mm to 40.22mm, in which the median is 7.6mm. The diameter distribution is shown in Fig. 6. Aneurysms in 3D data could be easily detected when they are larger than 4-5mm in diameter. But in 2D data, due to the occlusion, when the diameter of aneurysm is similar to that of the brain vessel, they cannot be clearly distinguished. For instance, aneurysms that occur on the artery as (a)(b) in Fig. 6 are less likely to be detected than those occur on arterial branch as (c)(d).

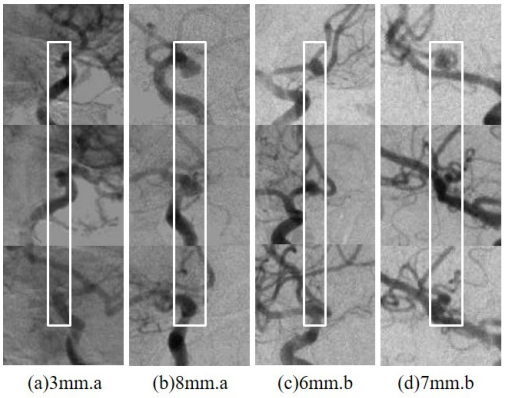

Fig. 7: Demonstration of aneurysms with different dimeter and position.(a) and (b) are aneurysms on vascular trunk with 3mm and 8mm in diameter; (c) and (d) are aneurysms on vascular branch with 6mm and 7mm in diameter.

IV. Experiment and Results

A. Experimental Setting

1) Data: 300 original sequences with 263 aneurysms were acquired. Among them 50 sequences are negative, and 8 sequences are with multiple aneurysms. Patients' angiograms and other clinical data were anonymized before analysis. The amount of ROIs to be concatenated per figure is empirically determined. The single-slice ROI with shape $250 * 250$ are extracted from original image with shape $1240*960$. The size of vertically connected images increases with the number of ROIs, in order not to oversize the data, we limit the number of ROIs to 3 to 6. All the SIF data were then augmented with horizontal and vertical flip, width and height shift and rotation with angle $90°$, $180°$ and $270°$, so that the number of training data expanded about sevenfold.

2) Evaluation index and experiment environment: For model performance evaluation, we adopt Accuracy, Precision, Sensitivity (also called as True Positive Rate(TPR) or Recall), Specificity (also called as True Negative Rate(TNR)), which are widely accepted as evaluation indexes in machine learning. All experiments are conducted on a computer with CPU Inter Core i5-8400 @ 2.80 GHz, GPU NVIDIA GeForce GTX 1050 Ti, and 16G of RAM.

$$precision = \frac{TP}{TP + FP} \tag{5}$$

$$sensitivity = recall = TPR = \frac{TP}{TP + FN} \tag{6}$$

$$specificity = TNR = \frac{TN}{FP + TN} \tag{7}$$

B. Experiment on SIF feature and Pre-processing

With the balance of the memory consumption and efficiency, we conducted experiments on SIF-5 comparing to the Non-SIF training data, which consists of single frame from the sequences as mentioned above. Also, the effect of noise reduction is given. As shown in the chart below, networks trained with filtered SIF data obtained better performance than that trained with Non-SIF or unfiltered data. All the data here have been augmented.

TABLE II: IMPACT OF SIF FEATURE AND NOISE REDUCTION ON VGG16 (%)

SIF	Acc.	TNR	TPR	Precision
Non-SIF	87.49	88.32	86.42	85.03
Non-SIF*	84.94	85.79	83.91	82.02
SIF-5	98.89	98.19	99.38	98.72
SIF-5*	97.39	96.79	97.84	97.61

* Without noise reduction.

The TABLE II shows the improvement of the accuracy with the filtered SIF feature. Noise reduction was less effective on augmented data than on un-augmented data, but still slightly improved the performance. Although the dimensions of the data themselves have not changed, the amount of information contained in a single image has multiplied. In terms of image size, the larger the image, within a certain range, the more information it contains. The third dimensional spatial information of the original imaging sequence is fused into the two-dimensional image, providing the network with the context information of aneurysm. Therefore, the task of aneurysm recognition is not limited to the traditional single image recognition or target detection,

This article has been accepted for publication in a future issue of this journal, but has not been fully edited. Content may change prior to final publication. Citation information: DOI 10.1109/TMI.2019.2951439, IEEE Transactions on Medical Imaging

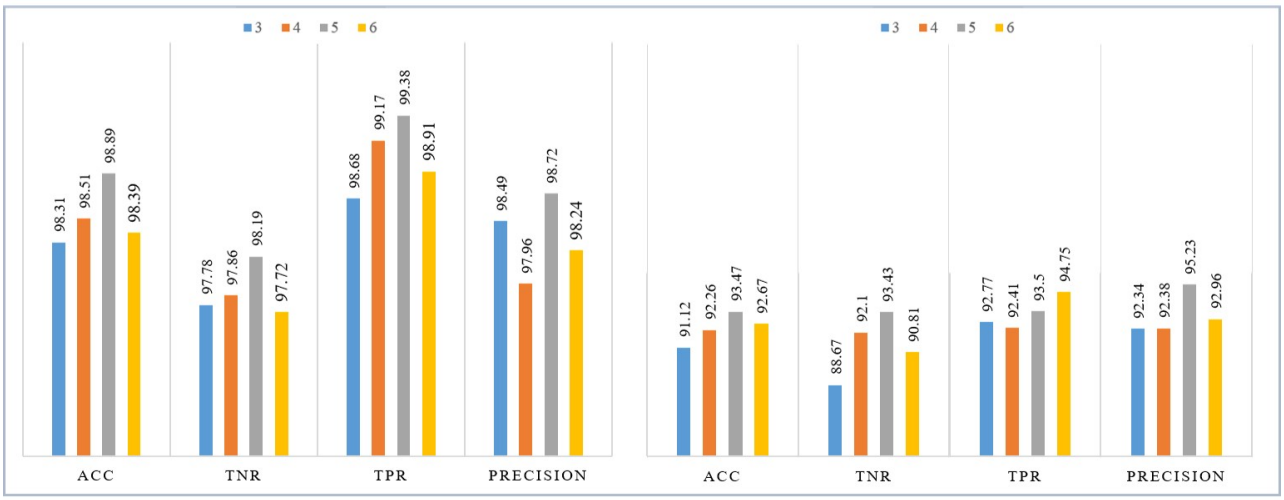

(a) Aug. (b) Non-Aug.

Fig. 8: Change in the detection accuracy, specificity(TNR), sensitivity(TPR) and precision of the proposed method for intracranial aneurysm under different SIF feature, which are presented in different colors. (a) and (b) are the networks trained with augmented data and non-augmented data, respectively.

but combined with the spatial information, which greatly improves the accuracy.

C. Experiment on data augmentation and SIF features

The most important difference between deep learning and traditional machine learning is that its performance increases with the amount of data. If the data are in limited quantities, then the performance of the deep learning algorithm could not be good as expected, which is because it needs a huge amount of data to understand the patterns contained therein. Since there exists little data available to the public, most medical image-based deep learning is limited by the size and breadth of the data. Therefore, it is critical to apply augmentation on data set.

In this part, we will study the influence of different SIF features on the detection results. In a single training image, the SIF features with different amount of consecutive ROIs range from three to six. The selection of the range is based on the aforementioned inter-frame angle difference and the rotational angle relationship between the proximal and distal aneurysms described in Fig. 5. When the amount of ROIs in the SIF feature exceeds a certain limit, we are prone to lose aneurysms in the latter ROIs, which will not be helpful for aneurysm detection. This is because with the increase in amount of single image, aneurysms may or may not appear in the latter ROIs of positive data. Meanwhile, the features of some overlaps of blood vessels are difficult to distinguish, so it is easy to confuse them with the features of small aneurysms. We explored the performance of aforementioned networks with and without data augmentation along with different SIF features, which are given in TABLE III.

As is depicted in Fig. 8 and TABLE III, there exists an overall trend that the network performance first improves and then degrades with the increase of SIF features. Although the precision of SIF-3 in Fig. 8 (a) and TPR of SIF-4 in (b) are slightly inconsistent with the trend, we can still conclude that the network would have a better performance

TABLE III: IMPACT OF DIFFERENT SIF FEATURES ON VGG16(%)

	Augmentation	Acc.	TNR	TPR	Precision
3	Aug.	98.31	97.78	98.68	98.49
	Non-aug.	91.12	88.67	92.77	92.34
4	Aug.	98.51	97.86	99.17	97.96
	Non-aug.	92.26	92.10	92.41	92.38
5	Aug.	**98.89**	**98.19**	**99.38**	**98.72**
	Non-aug.	93.47	93.43	93.50	95.23
6	Aug.	98.39	97.72	98.91	98.24
	Non-aug.	92.67	90.81	94.75	92.96

with SIF-5. When the number of SIF features contained in an image goes up, more dimensional information is included. Consequently, the accuracy has improved, which is consistent with our previous assumption. However, when it comes to SIF-6, the overall performance declines. We suppose that this is because there is a large angle difference between the first frame and the last frame of a batch of images where SIF features are extracted from. On the other hand, many aneurysms in the latter frames are lost, making the size of the single image increase without embedding more useful features.

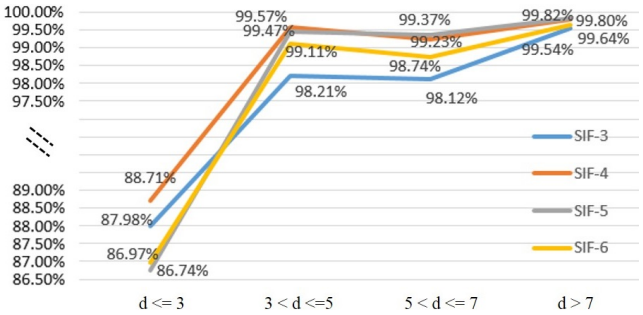

Fig. 9: The detection accuracy for aneurysms with different diameters under different SIF features on VGG16. d represents the diameter.

At the same time, since the size of aneurysms also has an impact on detection result, we made a quantitative evaluation to discuss the detailed relationship. As can be seen from Fig. 9 and TABLE IV, the detection accuracy

This article has been accepted for publication in a future issue of this journal, but has not been fully edited. Content may change prior to final publication. Citation information: DOI 10.1109/TMI.2019.2951439, IEEE Transactions on Medical Imaging

TABLE IV: THE DETECTION ACCURACY FOR ANEURYSMS WITH DIFFERENT DIAMETERS UNDER DIFFERENT SIF FEATURES ON VGG16 (%)

SIF	d<3	3<=d<5	5<=d<7	d>=7
SIF-3	87.98	98.21	98.12	99.54
SIF-4	88.71	99.57	99.23	99.80
SIF-5	86.74	99.47	99.37	99.82
SIF-6	86.97	99.11	98.74	99.64

of miniature aneurysm with diameter less than 3mm was relatively low, with an average level of 87.6%. When the aneurysm diameter was 3mm to 5mm, the average accuracy increased to 99.09%. When the aneurysm diameter further increased to 5mm to 7mm, the average accuracy decreased slightly to 98.84%. When the aneurysm diameter was larger than 7mm, the detection accuracy was improved to 99.7%.

Meanwhile, it can be found that when the aneurysm diameter was less than 3mm, the detection accuracy of SIF-5 and SIF-6 was lower than that of SIF-3 and SIF-4. This is consistent with our previous analysis that aneurysm features are more difficult to detect when the SIF features exceed a certain limit. Those redundant information increases as SIF features increase, and the available features will be overwhelmed by other information, so its accuracy declined instead. With the increase of aneurysm diameter, the detection accuracy of SIF-3 went lower than that of other SIF features, whereas the high detection accuracy of SIF-5 was basically consistent with the previous conclusion.

D. Model evaluation

In order to evaluate the proposed method, we use the original contrast sequences with 133 frames as the test data, which are in accord with the clinic. As mentioned above, the training data are 15 frames of images selected from the original data. However, this kind of sequences will not be used in clinic, and due to the large angle difference, those aneurysms which are more off-center are more likely to be lost in the latter frames. The original data size is 1240*960, with 133 frames in total, which means much unnecessary time would be cost when it's detected frame by frame since the angle difference between frames is only $1.36°$. Therefore, a process of original sequence-based intracranial aneurysm detection system is designed to fit the trained model, as given in Algorithm 1.

To ensure the accuracy, we set a random starting point $start$, namely skipping the first $start$ frames of the original 133-frame sequence. The value of $start$ does not need to be large, but can grow from the zero, that is, it is consistent with the frequency of detection. With each new starting point, a new test sequence is extracted from the original sequence and only few frames would be repetitively chosen. In this way we can test the same sequence multiple times without using the same sample.

In the previous experiment, the SIF-5 data reached the best results, so SIF-5 was used for test. We extracted 1 frame every 9 frames from the original 133-frame sequences, so 12 frames B were obtained per sequence as the first frames of 12 SIF-5 images. The remaining 13 frames were reserved for later SIF features. For each B_n, the computational area was further reduced to the region of the skull R_n, which can improve the computational efficiency. Then a series of preprocessing followed, and R_n was divided into 12 overlapping patched. To generate SIF-5 images, we set r_n^i in R_n as the first small ROI of SIF-5, and the R_n is the jth frame in S accordingly, where the boundary condition was $(m-1)(g+1) \leq k+133-n(k+1)-start$ so that SIF data would be generated on the last frame in R_n. Every g frames in S after R_n was chosen and a clipped image with the same position as r_n^i was taken as another small ROI in SIF-5. Finally, we detected the generated SIF image and then integrated the results.

Algorithm 1 The test on *Model* for aneurysm detection in original imaging sequence (with a shape of 1240*960*133)

Input: Original imaging sequence S (133 frames in total)
Output: Negative / Positive (if positive: return bounding box position (bbox))

Set a random starting position $start$ ($start \in 0, 1, 2, ...$). It can be set more than one time to achieve multiple detection without duplicate samples;
Choose a batch of frames B containing n frames: pick out 1 frame every k frame from S, so there would be $n = \lceil (133-start)/(k+1) \rceil$ frames in the batch;
Set $j = start + (n-1)(k+1) + 1$ as the actual position of B_n in original sequence S;
for $frame\ B_n\ in\ batch\ B$ **do**
    The region of patient's head R_n is segmented at a shape of 800*600 on the unsubtracted image to reduce scanning area and speed up calculation;
    Contrast control and noise reduction;
    Digital subtraction;
    12 overlapping patches $r_n^i (i = 1, 2, ..., 12)$ are extracted from R_n;
    for $patch\ r_n^i\ in\ R_n$ **do**
        To generate $SIF-m$ feature data, set a constant g as the number of frames that were skipped in S. Note that $(m-1)(g+1) \leq k+133-n(k+1)-start$. Then concatenate r_n^i, $r_{S_{j+g+1}}^i$, ..., $r_{S_{j+(m-1)(g+1)}}^i$ as c_n^i;
        Detection results $d_n^i \leftarrow Model(c_n^i)$.
        if $d_n^i == Positive$ **then**
            $bbox \leftarrow$ position i in frame n.
        end if
    end for
    if Positive results in $r_n^i \geq 3$ **then**
        This frame is positive.
    end if
end for
if Positive frames in $R_n^i \geq limit\ condition$ **then**
    This sequence is positive.
return bounding box
end if

The overlapping way do increase the cost of computation, but also prevents the aneurysm from being at the

This article has been accepted for publication in a future issue of this journal, but has not been fully edited. Content may change prior to final publication. Citation information: DOI 10.1109/TMI.2019.2951439, IEEE Transactions on Medical Imaging

TABLE V: COMPARISON WITH OTHER METHODS.

Method	Modality	Amount of Aneurysms	Size(mm)	Accuracy	Sensitivity	FP/case
CNN+distance mapping[28]	3D-DSA	21	-	-	100%	2.4
CNN+MIP[25]	TOF-MRA	508	2-5+	-	94.2%	2.9
Blobness filter+RF[27]	3D-DSA	10	-	-	76%	2.4
MLP+Haralick feature[31]	2D-DSA	47	6-21	98%	97%	-
Proposed method: CNN+SIF	2D-DSA	263	2-40	98.89%	99.37%	-

LDF: linear discriminant function. MIP: maximum intensity projection. MLP: multilayer perceptron. RF: random forest.

edge or corner of the image where cannot be detected normally. Meanwhile, due to the location of aneurysms, most aneurysms can be scanned by 4 patches in all locations, except those distal aneurysms which can only be scanned by 3 patches in a few locations like the edge of R_n. Therefore, if there are more than three positive sites in a same SIF image, we can consider that there is aneurysm in the intersection part of those overlapping areas. Note that there is a bounding box(bbox) in Algorithm 1, which is used to mark the position of aneurysm in each frame. In this way, we cannot only further screen and correct the wrong position according to this series of detected aneurysm position, but also provide radiologists with a visual feedback of the position information to improve efficiency.

V. Discussion

For the 12 SIF-5 images in the whole sequence, we can confirm the existence of aneurysms in the sequence when more than 7 of them are marked. The determination the limit conditions of 7 were obtained based on experiments (as shown in Fig. 10) and the following points: at the beginning and end of many angiography sequences, the contrast agent in the blood vessels was not in a filling state (Fig. 11(c)), thus many images did not have the characteristics of aneurysms at this stage. Secondly, since the inter-frame angle difference is around 4° in the test method, which is nearly four times than that of the training image, the smaller angle difference cannot avoid the occlusion or overlapping relationship in some cases. And finally we get an overall accuracy of 98% on original sequences, which can effectively provide radiologists with useful auxiliary diagnosis.

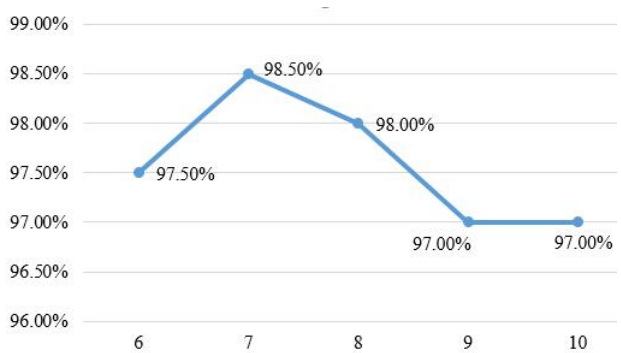

Fig. 10: Test accuracy under different limit condition. 200 sequences randomly selected from data set are used for test, and the limit condition are set from 6 to 10.

We have presented an efficient method for CAD system of intracranial aneurysm, and make a comparison with some other methods in TABLE V. The diameters of aneurysms range from 1.8mm to 40.22mm, in which the median is 7.6mm. It can be seen that we have a wide range in size and amount, covering different types and sizes of aneurysms, rather than the detection just saccular aneurysms as [31].

The proposed method is remarkably convincing, ensuring high accuracy and sensitivity under the large span of aneurysm size. However, the proportion of data distribution between the saccular aneurysm and the fusiform aneurysm is very unbalanced, and they were not been labeled by radiologists. On the other hand, the occurrence rate of the fusiform aneurysm is much lower than that of the saccular aneurysm, so the few training data lead to the poor performance of the network to detect the fusiform aneurysm with small diameter (Fig. 11(b)).

Since our detection is in the form of window sliding, it is less favorable for multiple aneurysms. If the distance between multiple aneurysms is large, which means they would be not likely to appear in the same window, we might get far more than four positive areas in the twelve overlapping patches. So in this situation we can detect multiple aneurysms as well as the single aneurysm. However, when two or more aneurysms are in adjacent area and the overlapping window is unable to scan them separately, it is difficult to get information of multiple aneurysms from CAD, which requires further diagnosis from radiologists. The improvement of this will be carried out in the next stage.

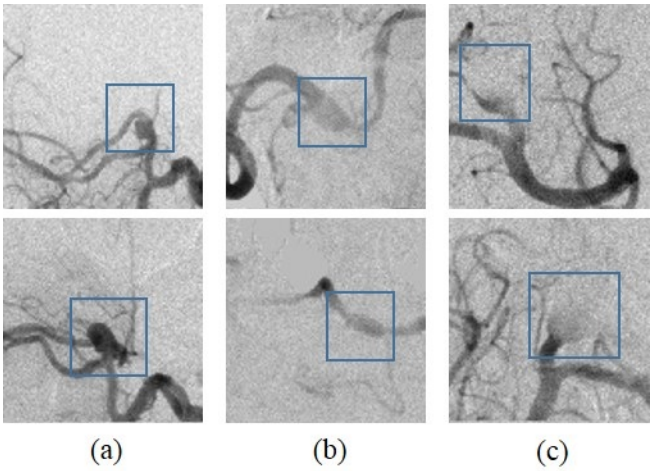

Fig. 11: Examples of saccular aneurysms (a), fusiform aneurysms (b) and aneurysms under incomplete angiography (c).

VI. Conclusion

Most studies on intracranial aneurysms focus on three-dimensional data such as MRA and CTA, which are relatively easy to process. However, DSA is still the gold

standard in the current aneurysm diagnosis. Therefore, we proposed a computer-assisted diagnosis method for intracranial aneurysm based on 3D-RA sequence that is not reconstructed. By integrating spatial information into two-dimensional data, we significantly improved the detection accuracy of single image. Finally, our method achieve 98.86% accuracy, 99.38% sensitivity and 98.19% specificity.

We first adjusted the brightness and contrast of sequences, and then performed digital subtraction and noise reduction. After that, we used the SIF feature images of sequence as the training data, and applied rapid transfer learning by slightly adjusting the structure of VGG16. In order to evaluate the effectiveness of SIF features, we studied the influence of SIF features at different scales, and further measured the performance on aneurysms with different sizes. Finally, we found that the SIF feature could effectively improve the detection accuracy of aneurysm to a certain extent, but after exceeding a limit, redundant information would be introduced and effective features of aneurysms would be overwhelmed. Therefore, the upper limit of scale should be carefully considered for different forms of data. In future work, we would further improve feature classification methods and the form of SIF features.

ACKNOWLEDGMENT

We acknowledge the efforts devoted by radiologists of the Beijing Tiantan Hospital to collect, label, and share the cerebral aneurysm database.

REFERENCES

[1] N. Chalouhi, B. L. Hoh, and D. Hasan, "Review of cerebral aneurysm formation, growth, and rupture," *Stroke*, vol. 44, no. 12, pp. 3613–3622, 2013.

[2] N. Ajiboye, N. Chalouhi, and R. M. Starke, "Unruptured cerebral aneurysms: Evaluation and management," *The Scientific World Journal,2015,(2015-6-4)*, vol. 2015, pp. 1–10, 2015.

[3] G. Kapsas, C. Budai, F. Toni, F. Patruno, A. F. Marliani, M. Leonardi, and et al., "Evaluation of CTA, time-resolved 4D CE-MRA and DSA in the follow-up of an intracranial aneurysm treated with a flow diverter stent," *Interventional Neuroradiology*, vol. 21, no. 1, pp. 69–71, 2015.

[4] Y. Hiratsuka, H. Miki, I. Kiriyama, K. Kikuchi, S. Takahashi, I. Matsubara, and et al., "Diagnosis of unruptured intracranial aneurysms: 3T MR angiography versus 64-channel multi-detector row CT angiography," *Magnetic Resonance in Medical Sciences*, vol. 7, no. 4, pp. 169–178, 2007.

[5] N. K. Yoon, S. McNally, P. Taussky, and M. S. Park, "Imaging of cerebral aneurysms: A clinical perspective," *Neurovascular Imaging*, vol. 2, no. 1, pp. 1–7, 2016.

[6] C. R. Regent, M. E. Goujon, D. Trystram, G. Boulouis, W. B. Hassen, S. G. Hardy, and et al., "Non-invasive diagnosis of intracranial aneurysms," *Diagn Interv Imaging*, vol. 95, no. 12, pp. 1163–1174, 2014.

[7] G. Litjens, T. Kooi, B. E. Bejnordi, A. A.Setio, F. Ciompi, M. Ghafoorian, and et al., "A survey on deep learning in medical image analysis," *Medical Image Analysis*, vol. 42, no. 9, pp. 60–88, 2017.

[8] R. Miotto, F. Wang, S. Wang, X. Jiang, and J. T. Dudley, "Deep learning for healthcare: Review, opportunities and challenges," *Briefings in Bioinformatics*, 2017.

[9] D. G. Shen, G. R. Wu, and H. Suk, "Deep learning in medical image analysis," *Annual Review of Biomedical Engineering*, vol. 19, no. 1, pp. 221–248, 2017.

[10] K. L. Ruedinger, D. R. Rutkowski, S. Schafer, A. R. Alzate, E. L. Oberstar, and C. Strother, "Impact of image reconstruction parameters when using 3D DSA reconstructions to measure intracranial aneurysms," *Journal of Neurointerventional Surgery*, vol. 10, no. 3, 2017.

[11] S. C. Wong, O. Nawawi, N. Ramli, and K. A. A. Kadir, "Benefits of 3D Rotational DSA Compared with 2D DSA in the evaluation of intracranial aneurysm," *Academic Radiology*, vol. 19, no. 6, pp. 701–707, 2012.

[12] W. Brinjikji, H. Cloft, G. Lanzino, and D. F. Kallmes, "Comparison of 2D digital subtraction angiography and 3D rotational angiography in the evaluation of dome-to-neck ratio," *Ajnr American Journal of Neuroradiology*, vol. 30, no. 4, p. 831, 2009.

[13] K. H. Yu, C. Zhang, G. J. Berry, R. B. Altman, C. Re, D. L. Rubin, and et al., "Predicting non-small cell lung cancer prognosis by fully automated microscopic pathology image features," *Nature Communications*, vol. 7, 2016.

[14] Y. Wang, F. Aghaei, A. Zarafshani, Y. Qiu, W. Qian, and B. Zheng, "Computer-aided classification of mammographic masses using visually sensitive image features," *Journal of X-Ray Science and Technology*, vol. 25, no. 1, pp. 1–16, 2017.

[15] R. Awan, N. A. Koohbanani, M. Shaban, A. Lisowska, and N. Rajpoot, "Context-aware learning using transferable features for classification of breast cancer histology images," in *International Conference Image Analysis and Recognition*, 2018, pp. 788–795.

[16] E. Arvaniti, K. S. Fricker, M. Moret, N. Rupp, T. Hermanns, C. Fankhauser, and et al., "Automated gleason grading of prostate cancer tissue microarrays via deep learning," *Scientific Reports*, vol. 8, 2018.

[17] V. Makde, J. Bhavsar, S. Jain, and P. Sharma, "Deep neural network based classification of tumourous and non-tumorous medical images," in *International Conference on Information and Communication Technology for Intelligent Systems*, 2017, pp. 199–206.

[18] J. Liu, F. Chen, C. Pan, M. Zhu, X. Zhang, L. Zhang, and et al., "A cascaded deep convolutional neural network for joint segmentation and genotype prediction of brainstem gliomas," *IEEE transactions on bio-medical engineering*, vol. PP, no. 99, pp. 1–1, 2018.

[19] Z. Yu, D. Ni, S. Chen, J. Qin, S. Li, T. Wang, and et al., "Hybrid dermoscopy image classification framework based on deep convolutional neural network and fisher vector," in *IEEE International Symposium on Biomedical Imaging*, 2017, pp. 301–304.

[20] D. Nie, R. Trullo, L. J. Lian, W. Li, C. Petitjean, R. Su, and et al., "Medical image synthesis with deep convolutional adversarial networks," *IEEE Transactions on Biomedical Engineering*, vol. PP, no. 99, 2018.

[21] Q. Dou, H. Chen, and L. Yu, "Multi-level contextual 3D CNNs for false positive reduction in pulmonary nodule detection," *IEEE Transactions on Biomedical Engineering*, vol. PP, no. 99, pp. 1–1, 2017.

[22] S. Chabert, T. Mardones, R. Riveros, M. Godoy, A. Veloz, R. Salas, and et al., "Applying machine learning and image feature extraction techniques to the problem of cerebral aneurysm rupture," vol. 3, 2017. DOI: 10.3897/rio.3.e11731.

[23] Z. Duan, Y. Li, S. Guan, C. Ma, Y. Han, X. Ren, and et al., "Morphological parameters and anatomical locations associated with rupture status of small intracranial aneurysms," *Scientific Reports*, vol. 8, no. 1, 2018.

[24] S. M. S1, N. Hayashi, Y. Masutani, Y. Nomura, T. Yoshikawa, S. Hanaoka, and et al., "Computer-assisted detection of cerebral aneurysms in MR angiography in a routine image-reading environment: Effects on diagnosis by radiologists," *American Journal of Neuroradiology*, vol. 37, no. 6, pp. 1038–1038, 2016.

[25] T. Nakao, S. Hanaoka, Y. Nomura, I. Sato, M. Nemoto, S. Miki, and et al., "Deep neural network-based computer-assisted detection of cerebral aneurysms in MR angiography," *Journal of Magnetic Resonance Imaging*, no. 1, 2017.

[26] C. M. Hentschke, O. Beuing, R. Nickl, and K. D. Tonnies, "Automatic cerebral aneurysm detection in multimodal angiographic images," in *Nuclear Science Symposium and Medical Imaging Conference*, 2011, pp. 3116–3120.

[27] T. Jerman, F. Pernus, and B. Likar, *Computer-Aided Detection and Quantification of Intracranial Aneurysms*. Springer International Publishing, 2015, pp. 3–10.

[28] T. Jerman, F. Pernus, B. Likar, and Z. Spiclin, "Aneurysm detection in 3D cerebral angiograms based on intra-vascular distance mapping and convolutional neural networks," in *IEEE International Symposium on Biomedical Imaging*, 2017, pp. 612–615.

[29] I. Rahmany and N. Khlifa, "Detection of intracranial aneurysm in angiographic images using fuzzy approaches," in *Image Processing, Applications and Systems Conference*, 2015, pp. 1–6.

[30] Y. Uchiyama, H. Ando, and R. Yokoyama, "Computer-aided diagnosis scheme for detection of unruptured intracranial aneurysms in MR angiography," in *International Conference of the Engineering in Medicine Biology Society*, 2005, pp. 3031–3031.

[31] K. M. Malik, S. M. Anjum, H. S. Zadeh, H. Malik, and G. M. Malik, "ISADAQ: A framework for intracranial saccular aneurysm detection and quantification using morphological analysis of cerebral angiograms," *IEEE Access*, no. 99, pp. 1–1, 2018.

[32] T. Jerman, F. Pernus, B. Likar, and Z. Spiclin, "Blob enhancement and visualization for improved intracranial aneurysm detection," *IEEE Transactions on Visualization Computer Graphics*, vol. 22, no. 6, pp. 1705–1717, 2016.

[33] C. M. Hentschke, K. D. Tonnies, O. Beuing, and R. Nickl, "A new feature for automatic aneurysm detection," in *IEEE International Symposium on Biomedical Imaging*, 2012, pp. 800–803.

[34] H. Hamdaoui, M. Maaroufi, B. Alami, M. Maaroufi, N. E. Chaoui, and S. Boujraf, "Computer-aided diagnosis systems for detecting intracranial aneurysms using 3D angiographic data sets: Review," in *International Conference on Advanced Technologies for Signal and Image Processing*, 2017, pp. 1–5.

[35] R. Yamashita, M. Nishio, R. K. G. Do, and K. Togashi, "Convolutional neural wetworks: An overview and application in radiology," *Insights Into Imaging*, pp. 1–19, 2018.

[36] H. C. Shin, H. R. Roth, M. Gao, L. Lu, Z. Xu, I. Nogues, and *et al*., "Deep convolutional neural networks for computer-aided detection: CNN architectures, dataset characteristics and transfer learning," *IEEE Transactions on Medical Imaging*, vol. 35, no. 5, pp. 1285–1298, 2016.